Atomic resolution structure of CAG RNA repeats: structural insights and implications for the trinucleotide repeat expansion diseases

Agnieszka Kiliszek, Ryszard Kierzek, Wlodzimierz J. Krzyzosiak and Wojciech Rypniewski*

Institute of Bioorganic Chemistry, Polish Academy of Sciences, Noskowskiego 12/14, 61-704 Poznan, Poland

ABSTRACT

CAG repeats occur predominantly in the coding regions of human genes, which suggests their functional importance. In some genes, these sequences can undergo pathogenic expansions leading to neurodegenerative polyglutamine (poly-Q) diseases. The mutant transcripts containing expanded CAG repeats possibly contribute to pathogenesis in addition to the well-known pathogenic effects of mutant proteins. We have analysed two crystal forms of RNA duplexes containing CAG repeats: $(GGCAGCAGCC)_2$. One of the structures has been determined at atomic resolution (0.95 Å) and the other at 1.9 Å. The duplexes include non-canonical A–A pairs that fit remarkably well within a regular A-helix. All the adenosines are in the *anti*-conformation and the only interaction within each A–A pair is a single $C2-H2 \cdots N1$ hydrogen bond. Both adenosines in each A–A pair are shifted towards the major groove, although to different extents; the A which is the H-bond donor stands out more (the 'thumbs-up' conformation). The main effect on the helix conformation is a local unwinding. The CAG repeats and the previously examined CUG structures share a similar pattern of electrostatic charge distribution in the minor groove, which could explain their affinity for the pathogenesis-related MBNL1 protein.

INTRODUCTION

Trinucleotide repeats have received special attention in biomedical research because some of them are known to undergo pathogenic expansions leading to incurable triplet repeat expansion diseases (TREDs) (1). Several TREDs are triggered by expanded triplet repeats located in UTRs of the implicated genes. These include fragile X syndrome (FXS) caused by abnormally elongated CGG repeats located in 5′-UTR of the fragile X mental retardation gene (*FMR1*), and myotonic dystrophy type 1 (DM1) caused by an expanded CUG repeat present in 3′-UTR of dystrophia myotonica protein kinase gene (*DMPK*). Most of the TREDs are triggered by expanded CAG repeat tracts that occur in protein-coding regions of specific single genes that are transcribed and translated into functionally unrelated proteins. The genetic diseases having this mutational basis include Huntington's disease, spinal and bulbar muscular atrophy (SBMA), dentatorubral-palidoluysian atrophy (DRPLA) and several spinocerebellar ataxias (SCAs). These disorders are also known under the common name of polyglutamine (poly-Q) diseases because the CAG repeat tracts encode polyglutamine, that results in altered protein structure, shown in numerous studies to be involved in pathogenesis (2,3).

Over this decade, several authors have proposed that also mutant transcript having expanded CAG repeat may contribute to pathogenesis of polyglutamine diseases (4–9). Among the arguments used in favour of this possibility was the similarity of the RNA secondary structure formed by the CAG repeats and CUG repeats implicated in RNA-mediated pathogenesis of DM1 and SCA8 (4,10). The CAG and the CUG repeats in transcripts have been shown to interact with the same splicing regulator MBNL1 (7,11) whose sequestration by CUG tracts cause alternative splicing aberrations leading to DM1 (12) and SCA8 (13). Moreover, it was shown using repeats expressed from suitable genetic constructs that expanded non-translated CAG repeats were capable of triggering neurodegeneration *in vivo* in the *Drosophila* eye model of SCA3 (8).

The CAG repeat tracts composed of six or more repeat units are present in about 300 human genes and these sequences are strongly overrepresented in exons, which suggests their positive selection and functional importance

*To whom correspondence should be addressed. Tel: +48 61 8528503; Fax: +48 61 8520532; Email: wojtekr@ibch.poznan.pl

(14). Little is known about physiological roles of CAG repeats in transcripts but their structural characterisation is more advanced. Most of the relevant structural studies have been carried out using biochemical methods on CAG repeats buried in sequence context of mRNAs of genes implicated in poly-Q disease (15–17). Short CAG repeat tracts were shown to be single-stranded, but longer repeats formed fairly stable hairpins in which alternating A–A interactions occurred between the G–C and C–G base pairs (18). Also structures formed by pure CAG repeats were compared with those formed by other triplet repeats, using both biochemical (10,20) and biophysical (19,20) methods. The CAG repeats were shown to form considerably more stable hairpins than CUG repeats of the same length (20) but the specific structural factor responsible for this difference could not be identified.

In this study, we have determined the crystal structure of an RNA duplex containing consecutive CAG repeats, based on two different crystal forms of GGCAGCAGCC. One of the structures has been determined at atomic resolution (0.95 Å). The study addresses the issue of the detailed structure as well as similarities and differences between the CAG and CUG repeat structures.

MATERIALS AND METHODS

Synthesis, purification and crystallization of CAG oligoribonucleotides

rGGCAGCAGCC oligomer was synthesized on an Applied Biosystems DNA/RNA synthesizer, using cyanoethyl phosphoramidite chemistry. Commercially available A, C and G phosphoramidites with 2'-*O*-tetrbutyldimethylsilyl were used for the synthesis of RNA (Glen Research, Azco, Proligo). The details of deprotection and purification of oligoribonucleotides were described previously (21). The RNA oligomer was dissolved in 100 mM KCl to the final concentration of 1 mM and annealed for 10 min at 65°C, then cooled slowly to ambient temperature within 2–3 h. Two forms of crystals were obtained, rhombohedral and trigonal, by the hanging drop/vapour diffusion method. The crystallization drops initially contained 2 μl of RNA and 2 μl of the reservoir solution. The initial volume of the reservoir solution was 500 μl. The rhombohedral crystal appeared after almost 1 year at 19°C in 25 mM MgSO₄, 50 mM Tris–HCl pH 8.5 and 1.8 M (NH₄)₂SO₄. The size of the crystal was 0.4 × 0.4 × 0.5 mm. The second form was obtained at 30°C in 10 mM MgSO₄, 50 mM cacodylate-NaOH pH 6.5 and 2 M (NH₄)₂SO₄. Crystals appeared within 2–3 weeks and then were moved to 19°C.

X-ray data collection, structure solution and refinement

X-ray diffraction data were collected: for the rhombohedral crystal on BL 14.1 beam line at the BESSY synchrotron in Berlin to the resolution of 0.95 Å and for the trigonal form on EMBL X13, DESY, Hamburg, resolution 1.9 Å. Both forms were cryoprotected by 20% glycerol (v/v) in the mother liquor. The data were integrated and scaled using the program suite DENZO/SCALEPACK (22). Although the cell parameters of the

two crystal forms were similar, the space groups were different: R32:H and P3₂ (details in Supplementary Data). Solving the structures by molecular replacement, using PHASER (23), revealed different packing of the r(GGC AGCAGCC)₂ oligomer in the same crystal cell. Early stages of the refinement were done using the program Refmac5 (24) from the CCP4 program suite (25) then refinement was carried out with PHENIX (26). Approximately 1000 reflections were set aside for the R_{free} statistic (5%). The program Coot (27) was used for visualisation of electron density maps $2F_o–F_c$ and $F_o–F_c$ and for manual rebuilding of the atomic model. Solvent water molecules were added by ARP/wARP (28) working in the default solvent building mode. During the refinement of the rhombohedral structure, anisotropic temperature factors was implemented and hydrogen atoms were added to the model. The last few cycles were performed using all data, including the R_{free} set. The final cycles of the refinement were carried out without stereochemical restraints. The trigonal model was refined using isotropic B-factors and TLS strategy.

The helical parameters were calculated using 3DNA (29). Sequence-independent measures were used, based on vectors connecting the C1′ atoms of the paired residues, to avoid computational artefacts arising from non-canonical base pairing. Program PDB2PQR (30) was used to assign partial charges and radii to atoms of the models, according to the AMBER force field. Subsequently, the surface electrostatic potential for the RNA models was calculated with APBS (31). All pictures were drawn using PyMOL v0.99rc6 (32). The coordinates of both crystallographic models have been deposited with the Protein Data Bank (PDB). The accession codes are 3NJ6 and 3NJ7.

RESULTS

Final models

In the rhombohedral structure, the asymmetric unit contains one RNA strand (chain H). The second strand of the duplex is symmetry-related *via* a crystallographic 2-fold axis. In the trigonal structure, the asymmetric unit contains tree duplexes: A+B, C+D, E+F. All the duplexes stack end-to-end, forming semi-infinite columns parallel to the *c* cell edge. The RNA interacts with ordered water molecules and sulphate anions. The models are summarized in Table 1 and Supplementary Table S1. Crystal lattice interactions are discussed in Supplementary Data.

RNA duplex conformation and non-canonical A-A pairing

The sequence-independent helical parameters, based on inter-strand vectors between C1′ atoms, were found to be a convenient, although simplified, measure of the helix properties (Supplementary Table S2). All the duplexes are in the A-form, with the Z_p values (the displacement of the phosphorus atom from the *xy*-plane of the 'middle frame' between neighbouring base-pairs) in the range 2.3–3.1 Å (33). The sugar conformation of most residues is 3′-*endo,* with the exception of 5G in

Table 1. Summary of the atomic models and refinement statistics of (GGCAGCAGCC)$_2$

Crystal form	R32:H	P3$_2$
Resolution (Å)	0.95	1.9
Overall mean B-factor (Å^2)	11.4	24.4
Number of reflections: work/test	21 748	15 413/821
R-value (%)	10.6	21.17
R-free (%)	–	24.82
RNA atoms	213	1278
Water molecules	86	170
No. sulphate ions	1	6
R.m.s.d. in bonds (Å)	0.016	0.006
R.m.s.d. in angles (°)	2.0	1.4

chain A and 5G in chain E, which show the 2'-*exo* puckering. Values of the torsion angles fit in the typical range for the A-form (Supplementary Table S3). However, some distortions are observed, mainly for α- and γ-angles of all guanosines 5G. Instead of the common A-RNA conformation –*gauche* –*sc*, the α-angles for 5G in all seven strands are in different conformational regions: +*sp* for chain H, +*ac* for chain A, C and E, –*ac* for B, D and F. Only in chain B the γ-angle is in the typical +*sc*. It is +*ap* in H, –*ap* in A, C and E, +*ac* in D and F. This can be visualized as flipping of the O5' atom due to a rotation of the O5'–C5' bond. The effect on the conformation of the RNA strand is that the sugar rings of 5G and 4A become nearly co-planar (Figure 1). The corresponding helical twist shows unwinding of the duplex in the AG/CA steps, with helical twist values in the range 18–22°, compared to an average of 31° for other steps. Overall, the duplexes are underwound with average values of 12.5–12.9 base pairs per turn. The major groove opens up in the middle of each duplex to >20 Å (Supplementary Table S4). The inter-strand distance measured between the C1' atoms of the paired residues is typical for A-RNA—10.7 Å, with standard deviation of 0.2 Å. It is only slightly longer (11.0 Å) for the paired adenosines.

All the base pairs are well defined in the electron density and the atomic temperature factors do not show any clear patterns of variability along the RNA sequence. The C–G pairs show the Watson–Crick interactions. All the adenosines are in the *anti* conformation and the only interaction within each A–A pair is a single C2-H2···N1 hydrogen bond (Figure 2). In the rhombohedral, atomic resolution structure, the distance between C2 and N1 is 3.41 Å. When the H2 atom is included in the riding position its distance to N1 is 2.44 Å, which is closer by 0.3 Å than the sum of their van der Waals radii. The C, H and N atoms are almost co-linear (bond angle = 176°). Consistently with the atomic resolution data, the distances between C2 and N1 in the trigonal structure are in the range 3.1–3.4 Å. Of the two conformations that are possible in each A–A pair, the adenosine closer to the 3'-end is shifted towards the major groove, as indicated by the λ-angle (87° on average) between the bond C1'–N9 and the line between the C1' atoms of the paired residues. The other adenosine is also upturned (λ = 64°) compared to

the other residues in both structures (average λ = 55° in the range 51–58°).

Stacking interaction

Three kinds of stacking interactions are observed in both structures: one for the GC/GC step and two for the CA/AG step, depending on the conformation of the adenosines (Figure 3). The Watson–Crick pairs show extensive overlaps typical for canonical base pairs. Reduced stacking is observed for steps involving non-canonical pairing. The more upturned adenosines stack with adjacent cytosines, on the 5' side (average of overlap area 2.2 ± 1.1 Å^2), but are far removed and do not stack with guanosines adjacent on the 3'-side. The less upturned adenosines stack to a certain degree with both their adjacent residues (0.8 ± 0.1 Å^2 with C and 0.3 ± 0.3 Å^2 with G).

Hydration, ions and intermolecular interactions

The hydration of the A–A pairs forms a pattern similar in all the duplexes in the two crystal forms. In the minor groove, there is a single water molecule associated with each adenosine, bridging N3 with the O2' atom of the ribose ring. In the major groove, there is usually a water molecule associated with N7. A sulphate ion is wedged between the paired adenine rings. One oxygen atom (O1) of the sulphate ion interacts simultaneously with N6 of the less upturned (towards the major groove) adenosine and with N1 of the other base. Another sulphate oxygen (O2) interacts with N6 of the same base (Figure 2). The interaction with the sulphate can be described as a merging of the anion binding sites described as ADE_WC_H and ADE_WC (34). The occupancy factor of the sulphate ion is ~0.5. In its absence, a water molecule occupies the position of O1.

The hydration of C–G pairs also shows regularity, especially in the high-resolution structure. In the major groove, guanosines interact with two or three water molecules. There are always two water molecules H-bonded with the O6 and N7 atoms. The third is associated with the phosphate group. There are one or two water molecules associated with the cytosines in the major groove. One always interacts with the *exo*-amino group and the other is bound to the phosphate. In the minor groove, the guanosines have the capacity to interact with two water molecules: one at the *exo*-amino group, the other between the N3 atom and the ribose ring. However, in two cases, one of the water molecule is displaced by H-bonds formed with the oxygen atom of a symmetry-related residue. Cytosines each have one water molecule in the minor groove, H-bonded to the O2 atom.

In the trigonal lattice, there are six ribose–ribose intermolecular interactions, each consisting of four CH···O hydrogen bonds: two C1'-H1'···O2' and two C4'-H4'···O4'. Every 3C and every 8G is involved, on each strand. The paired sugars are either between two cytidines (two pairs), two guanosines (two pairs) or between a cytidine and a guanosine (two pairs). Similarly, in the rhombohedral structure, two symmetry-related pairs are
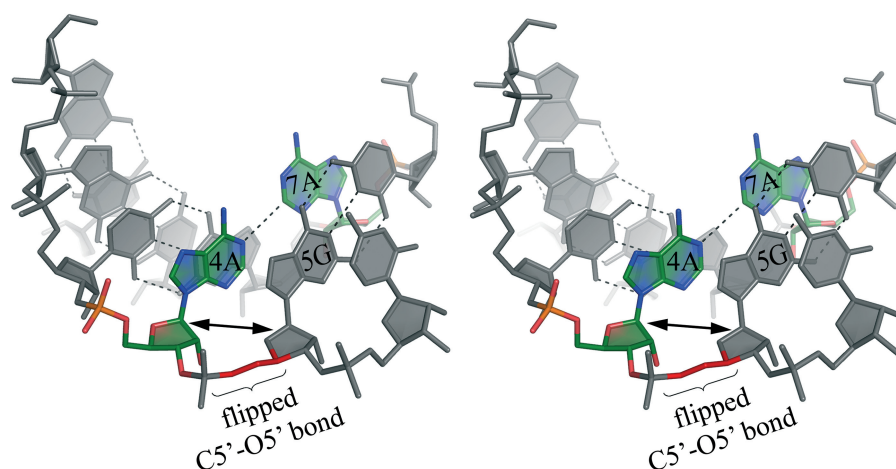
Figure 1. Stereo view of the A–A pair (green) and its surroundings in the (GGCAGCAGAA)$_2$ 0.95 Å resolution structure. The α- and γ-backbone torsion angles between A4 and G5 take unusual values (see text) which results in local unwinding of the helix. This can be seen by comparing the orientation of consecutive ribose rings, which appear co-planar in the two residues. This conformation of the backbone is found in all the examined A–A pairs and is associated with the adenosine less inclined towards the major groove.
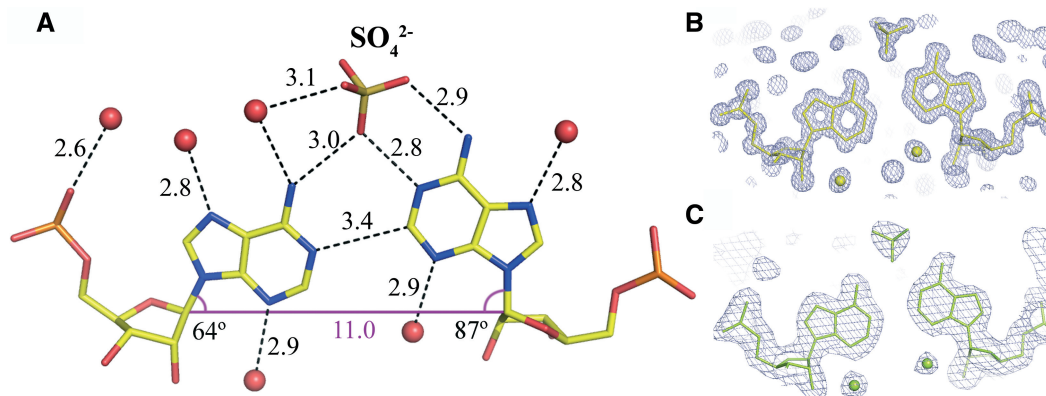

Figure 2. The A–A pair and its solvation. (**A**) The CH···N bond between the adenine rings is found in all the examined pairs. An associated sulphate anion is always found in the major groove but its occupancy factor is ~0.5. The λ-angles are shown indicating the inclination of the residues towards the major groove. One adenine ring is always elevated more than the other and both are higher than average found for the C–G base pairs. The corresponding $2F_o–F_c$ electron density is shown for the rhombohedral (**B**) and a representative density for the trigonal structure (**C**).

observed of 3C with 8G (Supplementary Figure S2). The average donor-acceptor distance is 3.4 Å with the standard deviation 0.1 Å.

Electrostatic potential and surface features

The calculated electrostatic potential shows a similar surface charge distribution for all duplexes. In the minor groove, the bands of positive and negative charge are arranged alternately along the direction of the helix axis (Figure 4). The positive bands are formed by the sugar rings and the *exo*-amino groups of G. The major groove is predominantly electronegative with patches of positive potential at the stacked A and C residues. The hydrogen atoms of the amino groups of each A–A pair form a stripe of electropositive potential across the major groove. These are the binding places of the sulphate ions. Adjacent cytosines generate additional positive patches on either side of the A–A pair, while the adjacent guanosines form electronegative niches in the surface of the major groove. The large shift between A and G, leading to

their unstacking, results in characteristic surface features in both grooves: an indentation in the minor groove due to the protruding adenosine and a corresponding niche in the major groove at the adjacent (on the 3′-side) guanosine.

DISCUSSION

This work is part of the project to determine high-resolution crystal structures of all four CNG repeats, in order to identify their common and distinguishing features, which can then be interpreted in terms of their function. The atomic model interpreted in the context of the known physiochemical properties, such as the ligand affinity, surface features, electrostatic profile or hydrogen-bonding network and hydration can be used in ligand design.

One distinguishing feature of the presented structures is the A–A wobble, which to our knowledge has not been observed before. One other example of A–A pairing is found within the ribosome model (pdb code 1FFK) (35), in which both residues are in the *anti* conformation and
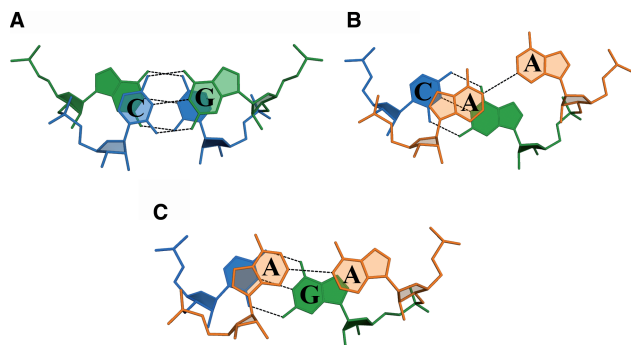
Figure 3. Stacking interactions in the GC/GC step (**A**) and two kinds of CA/AG (**B** and **C**) depending on the conformation of the A–A pair.
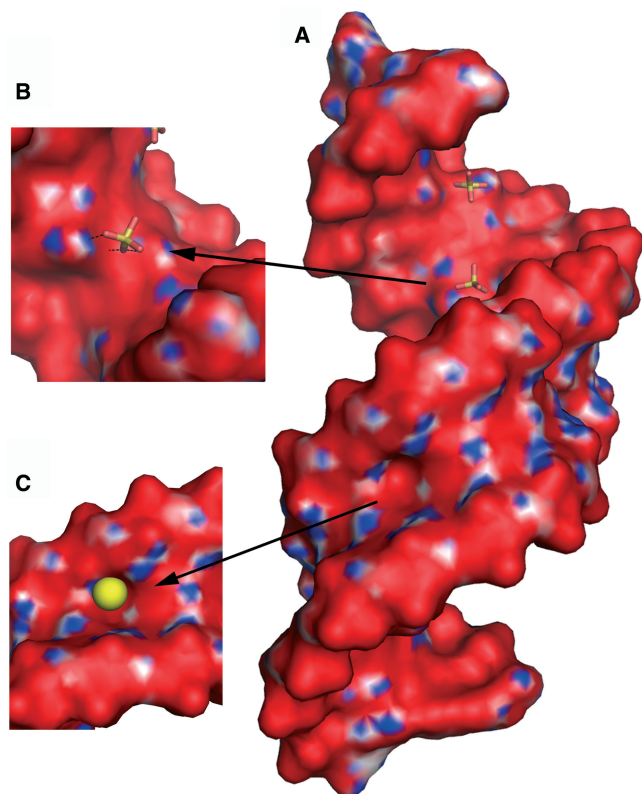

Figure 4. The electrostatic potential surface for (**A**) the rhombohedral structure, showing two consecutive duplexes. Red is negative, blue is positive. Sulphate anions (sticks) are shown interacting in the major groove (detailed in **B**). A distinct cavity in the minor groove is filled by a water molecule (yellow sphere in **C**).

interact with their Watson–Crick edges within an irregular double-stranded structure. However, the details of their interactions are different: the N6 amino group is H-bonded with N1, the two adenine rings are far from co-planar and it is doubtful if there is any significant interaction between N1 and C2 (distance 3.7 Å). The C1'–C1' distance in the ribosomal structure is 12.4 Å—a consequence of the large size of the two purines interacting *vis-a-vis*. In contrast, the A–A pairs presented here, embedded in CAG repeats, fit remarkably well within a regular A-helix. Although accommodation of the

interacting purine rings seems to be sterically demanding, the inter-strand C1'–C1' distances for the adenosine residues are only slightly larger than average. This ability to conform to the helical form is worth noting in view of the fact that in the literature the CNG double stranded forms are often referred to as 'containing internal loops'. In terms of the 3D structure, the main consequence of an A–A pair seems to be a local unwinding of the duplex. For the adenosine that is inclined towards the minor groove, the α-torsion angle of the following G takes positive or high negative values, and γ takes high values (Figure 1, Supplementary Table S3). Consequently, the two sugar rings on either side of the phosphate group are almost co-planar, as opposed to the typical case, in which the successive sugar rings follow the helical twist. The values of the twist associated with A–A and the following pair are small (in the range 18–22°) compared with the average value of 31–32° for other steps in the duplexes.

The only interaction between the paired adenosine residues is the weak C2-H2···N1 bond. Carbon is a poorer donor than nitrogen or oxygen and the later two clearly dominate in the H-bonding interactions in biological molecules. The energy of C-H···X bonds is estimated to be ∼1 kcal/mol or less, with the C-H···N bonds being weaker, less frequent and poorly studied compared to C-H···O. The energies, although small, are not negligible and correspond to measurable effects on the thermal stability of the duplex. Remarkably, in a thermodynamic study of related RNA sequences (19), bromination of one adenine, which is expected to force the adenosine residue into the *syn* conformation, results in a destabilisation of the helix, as indicated by an increase of the free energy of duplex formation by ∼0.7 kcal/mol, with a decrease of the melting temperature by a corresponding 4°C. The effect seems to be additive when more A–A pairs are modified.

In order to assess the biological significance, one needs to consider the present structure in the wider context of CNG repeats. Pathogenesis involving expanded runs of CAG repeats is well known to occur at the protein level. However, the role of the transcripts should also be considered. In one type of spinocerebellar ataxia the abnormal CAG run is found only in the UTR, the 5'-UTR promoter (36). In binding studies of MBNL1 protein, CAG repeats show similar affinity as CUG runs, both *in vitro* and *in vivo* (7,11,37). Detailed and well-parameterized structural model is necessary to explain the physiochemical properties of CAG structures and to use them as targets for ligands to block the translation of poly-Q mutant proteins. When comparing the present structure of the CAG repeats and the previously described CUG repeats (38) one can observe both similarities and differences (Table 2 and Supplementary Figures S3–5). In terms of the overall helical twist the CAG-containing duplexes are underwound (12.5–12.9 bp/turn), while CUG structures are more typical (11 bp/turn). The major groove in the CAG helices is wide and shallow, while in CUG it is narrow and deep. Each A–A and U–U pair can assume two alternative relative positions, depending on which base is the H-bond donor or acceptor (as it happens, the acceptor

Table 2. Comparison of characteristic features of double helical CAG and CUG (38) repeats

Feature	CAG	CUG
Helix form	A	A
Helical twist[a] (°)	28.5 ± 5.7	33.6 ± 4.1
Major groove width[b] (Å)	23.8 ± 0.2	12.7 ± 2.3
Minor groove width[b] (Å)	15.3 ± 0.1	15.7 ± 0.4
Average C1′–C1′ distance for *N–N*[c] (and for the other pairs) (Å)	11.0 (10.7)	10.4 (10.5)
Local effect of *N–N* on helicity	unwinding	not observed
N–N pairing interaction	C2-H2···N1 hydrogen bond	N3-H3···O4 hydrogen bond
Manner of accommodating *N–N* (according to direction of the glycosidic bond, λ)	One A turned towards major groove ('thumbs-up')	One U inclined towards minor groove
Effect of *N–N* conformation on neighbouring *N–N*	Cooperativity: A–A pairs in consecutive repeats have alternative conformations	No effect: each U–U takes one of two possible conformation independently
Electrostatic profile	Alternating stripes of positive and negative potential due to C–G pairs	Alternating stripes of positive and negative potential due to C–G pairs
Observed ligand affinity of *N–N*	Sulphate binding in major groove	Sulphate or glycerol through-water binding in major groove
Exposed functional groups of *N–N*		
Major groove	First A N6 amino Second A N1 imino, N6 amino	First U O4 carbonyl

Minor groove	First A N3 imino
	   Second A N3 imino
		First U O2 carbonyl
		   Second U O2 carbonyl, N3 amino

[a]Average for A-RNA is 33.1 (39).
[b]The values given are the 'refined' widths, according to the program 3DNA (29).
[c]A–A or U–U base pair.

in both types of repeat is more inclined towards the minor groove). The four CAG-containing duplexes in the two crystal structure are closely superposable and they all show the same order of A–A paring conformations. The first adenosine, from the 5′-end, always acts as the H-bond acceptor within the A–A pair and the second A is in the 'thumbs-up' conformation, pointing towards the major groove, and acts as the H-bond donor. This is not a consequence of crystal symmetry, at least in the case of the trigonal structure, in which the three duplexes are crystallographically independent. The observed structures all correspond to one of three theoretically foreseeable arrangements of two consecutive A–A pairs (the other, unobserved, arrangements of the two adenosines within a strand would have alternating but reversed inclinations or similar inclinations). This can be contrasted with the structure of (CUG)$_n$ duplexes which show an apparently random order of two possible U–U pairing conformations within the CUG repeats (38).

One clear similarity between CAG- and CUG-duplexes is the pattern of stripes of alternating positive and negative electrostatic potential in the minor groove. The structural basis of the pattern is similar in both types of repeats except that the negative potential in the CAG structure is due to the imine groups of the adenosine residues, while in the CUG structure this is due to the carbonyl oxygen atoms of the uridines. This could explain some features of the repeat tracts, such as the reported affinity of the MBNL1 protein for both CUG and CAG (38). In the case of CCG repeats (whose structure is still unknown), which are also recognized by the MBNL1 protein, the C–C pairs should also contribute electronegative potential in the minor groove, due to their carbonyl groups. In contrast, the CGG-containing duplexes, which do not interact directly with the MBNL1 protein (40), are

expected to present in the minor groove at least one prominent amine group. In the major groove, on the other hand, the A–A pair shows an affinity for sulphate ions. This is apparently due to the exposed Watson–Crick edge of the adenosine in the 'thumbs-up' conformation. The binding of the sulphate is a consequence of high concentration of the anions in the crystallization medium and is unlikely to take place to a significant degree in the cell, but the interaction in the crystals can be taken as an indication of an affinity of the exposed Watson–Crick edge of the adenine for negatively charged bidentate ligands.

ACCESSION NUMBERS

The accession numbers are PDB 3NJ6, 3NJ7.

SUPPLEMENTARY DATA

Supplementary Data are available at NAR Online.

FUNDING

Conflict of interest statement. None declared.

REFERENCES

1. Orr,H.T. and Zoghbi,H.Y. (2007) Trinucleotide repeat disorders. *Annu. Rev. Neurosci.*, **30**, 575–621.
2. La Spada,A.R. and Taylor,J.P. (2010) Repeat expansion disease: progress and puzzles in disease pathogenesis. *Nat. Rev. Genet.*, **11**, 247–258.
3. Zoghbi,H.Y. and Orr,H.T. (2009) Pathogenic mechanisms of a polyglutamine-mediated neurodegenerative disease, spinocerebellar ataxia type 1. *J. Biol. Chem.*, **284**, 7425–7429.
4. Galvão,R., Mendes-Soares,L., Câmara,J., Jaco,I. and Carmo-Fonseca,M. (2001) Triplet repeats, RNA secondary structure and toxic gain-of-function models for pathogenesis. *Brain Res. Bull.*, **56**, 191–201.
5. Broude,N.E. and Cantor,C.R. (2003) Neurological diseases and RNA-directed gene regulation: prospects for new diagnostics and therapy. *Expert Rev. Mol. Diagn.*, **3**, 269–274.
6. Jasinska,A., Michlewski,G., de Mezer,M., Sobczak,K., Kozlowski,P., Napierala,M. and Krzyzosiak,W.J. (2003) Structures of trinucleotide repeats in human transcripts and their functional implications. *Nucleic Acids Res.*, **31**, 5463–5468.
7. Ho,T.H., Savkur,R.S., Poulos,M.G., Mancini,M.A., Swanson,M.S. and Cooper,T.A. (2005) Colocalization of muscleblind with RNA foci is separable from mis-regulation of alternative splicing in myotonic dystrophy. *J. Cell Sci.*, **118**, 2923–2933.
8. Li,L.-B., Yu,Z., Teng,X. and Bonini,N.M. (2008) RNA toxicity is a component of ataxin-3 degeneration in Drosophila. *Nature*, **453**, 1107–1111.
9. Birman,S. (2008) Neurodegeneration: RNA turns number one suspect in polyglutamine diseases. *Curr. Biol.*, **18**, R659–R661.
10. Sobczak,K., de Mezer,M., Michlewski,G., Krol,J. and Krzyzosiak,W.J. (2003) RNA structure of trinucleotide repeats associated with human neurological diseases. *Nucleic Acids Res.*, **31**, 5469–5482.
11. Yuan,Y., Compton,S.A., Sobczak,K., Stenberg,M.G., Thornton,C.A., Griffith,J.D. and Swanson,M.S. (2007) Muscleblind-like 1 interacts with RNA hairpins in splicing target and pathogenic RNAs. *Nucleic Acids Res.*, **35**, 5474–5486.
12. Miller,J.W., Urbinati,C.R., Teng-Umnuay,P., Stenberg,M.G., Byrne,B.J., Thornton,C.A. and Swanson,M.S. (2000) Recruitment of human muscleblind proteins to (CUG)(n) expansions associated with myotonic dystrophy. *EMBO J.*, **19**, 4439–4448.
13. Daughters,R.S., Tuttle,D.L., Gao,W., Ikeda,Y., Moseley,M.L., Ebner,T.J., Swanson,M.S. and Ranum,L.P.W. (2009) RNA gain-of-function in spinocerebellar ataxia type 8. *PLoS Genet.*, **5**, e1000600.
14. Kozlowski,P., de Mezer,M. and Krzyzosiak,W.J. (2010) Trinucleotide repeats in human genome and exome. *Nucleic Acids Res.*, **38**, 4027–4039.
15. Michlewski,G. and Krzyzosiak,W.J. (2004) Molecular architecture of CAG repeats in human disease related transcripts. *J. Mol. Biol.*, **340**, 665–679.
16. Sobczak,K. and Krzyzosiak,W.J. (2004) Imperfect CAG repeats form diverse structures in SCA1 transcripts. *J. Biol. Chem.*, **279**, 41563–41572.
17. Sobczak,K. and Krzyzosiak,W.J. (2005) CAG repeats containing CAA interruptions form branched hairpin structures in spinocerebellar ataxia type 2 transcripts. *J. Biol. Chem.*, **280**, 3898–3910.
18. Krzyzosiak,W.J., Sobczak,K. and Napierala,M. (2006) In Wells,R.D. (ed.), *Genetic Instabilities and Neurological Diseases*. Elsevier, pp. 705–716.
19. Broda,M., Kierzek,E., Gdaniec,Z., Kulinski,T. and Kierzek,R. (2005) Thermodynamic stability of RNA structures formed by CNG trinucleotide repeats. Implication for prediction of RNA structure. *Biochemistry*, **44**, 10873–10882.
20. Sobczak,K., Michlewski,G., de Mezer,M., Kierzek,E., Krol,J., Olejniczak,M., Kierzek,R. and Krzyzosiak,W.J. (2010) Structural diversity of triplet repeat RNAs. *J. Biol. Chem.*, **285**, 12755–12764.
21. Xia,T., SantaLucia,J. Jr, Burkard,M.E., Kierzek,R., Schroeder,S.J., Jiao,X., Cox,C. and Turner,D.H. (1998) Thermodynamic parameters for an expanded nearest-neighbor model for formation of RNA duplexes with Watson-Crick base pairs. *Biochemistry*, **37**, 14719–14735.
22. Otwinowski,Z. and Minor,W. (1997) Processing of X-ray diffraction data collected in oscillation mode. *Methods Enzymol.*, **276**, 307–325.
23. Storoni,L.C., McCoy,A.J. and Read,R.J. (2004) Likelihood-enhanced fast rotation functions. *Acta Crystallogr. D Biol. Crystallogr.*, **60**, 432–438.
24. Murshudov,G.N., Vagin,A.A. and Dodson,E.J. (1997) Refinement of macromolecular structures by the maximum-likelihood method. *Acta Crystallogr. D Biol. Crystallogr.*, **53**, 240–255.
25. Collaborative Computational,P. (1994) The CCP4 suite: programs for protein crystallography. *Acta Crystallogr. D Biol. Crystallogr.*, **50**, 760–763.
26. Adams,P.D., Grosse-Kunstleve,R.W., Hung,L.W., Ioerger,T.R., McCoy,A.J., Moriarty,N.W., Read,R.J., Sacchettini,J.C., Sauter,N.K. and Terwilliger,T.C. (2002) PHENIX: building new software for automated crystallographic structure determination. *Acta Crystallogr. D Biol. Crystallogr.*, **58**, 1948–1954.
27. Emsley,P. and Cowtan,K. (2004) Coot: model-building tools for molecular graphics. *Acta Crystallogr. D Biol. Crystallogr.*, **60**, 2126–2132.
28. Lamzin,V.S. and Wilson,K.S. (1993) Automated refinement of protein models. *Acta Crystallogr. D Biol. Crystallogr.*, **49**, 129–147.
29. Olson,W.K., Bansal,M., Burley,S.K., Dickerson,R.E., Gerstein,M., Harvey,S.C., Heinemann,U., Lu,X.J., Neidle,S., Shakked,Z. *et al.* (2001) A standard reference frame for the description of nucleic acid base-pair geometry. *J. Mol. Biol.*, **313**, 229–237.
30. Dolinsky,T.J., Nielsen,J.E., McCammon,J.A. and Baker,N.A. (2004) PDB2PQR: an automated pipeline for the setup of Poisson-Boltzmann electrostatics calculations. *Nucleic Acids Res.*, **32**, W665–W667.
31. Baker,N.A., Sept,D., Joseph,S., Holst,M.J. and McCammon,J.A. (2001) Electrostatics of nanosystems: application to microtubules and the ribosome. *Proc. Natl Acad. Sci. USA*, **98**, 10037–10041.
32. DeLano,W.L. (2002) *The PyMOL Molecular Graphics System*. DeLano Scientific, Palo Alto, CA, USA.
33. Lu,X.-J. and Olson,W.K. (2003) 3DNA: a software package for the analysis, rebuilding and visualization of three-dimensional nucleic acid structures. *Nucleic Acids Res.*, **31**, 5108–5121.
34. Auffinger,P., Bielecki,L. and Westhof,E. (2004) Anion binding to nucleic acids. *Structure*, **12**, 379–388.
35. Ban,N., Nissen,P., Hansen,J., Moore,P.B. and Steitz,T.A. (2000) The complete atomic structure of the large ribosomal subunit at 2.4 A resolution. *Science*, **289**, 905–920.
36. Todd,P.K. and Paulson,H.L. (2010) RNA-mediated neurodegeneration in repeat expansion disorders. *Ann. Neurol.*, **67**, 291–300.
37. Kino,Y., Mori,D., Oma,Y., Takeshita,Y., Sasagawa,N. and Ishiura,S. (2004) Muscleblind protein, MBNL1/EXP, binds specifically to CHHG repeats. *Hum. Mol. Genet.*, **13**, 495–507.
38. Kiliszek,A., Kierzek,R., Krzyzosiak,W.J. and Rypniewski,W. (2009) Structural insights into CUG repeats containing the 'stretched U-U wobble': implications for myotonic dystrophy. *Nucleic Acids Res.*, **37**, 4149–4156.
39. Bloomfield,V.A., Crothers,D.M. and Tinoco,I. (2000) *Nucleic Acids: Structures, Properties, and Functions*. University Science Books, Sausalito.
40. Sellier,C., Rau,F., Liu,Y., Tassone,F., Hukema,R.K., Gattoni,R., Schneider,A., Richard,S., Willemsen,R., Elliott,D.J. *et al.* (2010) Sam68 sequestration and partial loss of function are associated with splicing alterations in FXTAS patients. *EMBO J.*, **29**, 1248–1261.